Neuroimaging

# Utility of perfusion PET measures to assess neuronal injury in Alzheimer's disease

Nelly Joseph-Mathurin[a], Yi Su[b,*], Tyler M. Blazey[a], Mateusz Jasielec[c], Andrei Vlassenko[a], Karl Friedrichsen[a], Brian A. Gordon[a], Russ C. Hornbeck[a], Lisa Cash[a], Beau M. Ances[d], Thomas Veale[e], David M. Cash[e], Adam M. Brickman[f], Virginia Buckles[d], Nigel J. Cairns[d], Carlos Cruchaga[g], Alison Goate[h], Clifford R. Jack, Jr.[i], Celeste Karch[d], William Klunk[j], Robert A. Koeppe[k], Daniel S. Marcus[a], Richard Mayeux[f], Eric McDade[d], James M. Noble[f], John Ringman[l], Andrew J. Saykin[m], Paul M. Thompson[n], Chengjie Xiong[c], John C. Morris[d], Randall J. Bateman[d], Tammie L. S. Benzinger[a], and the Dominantly Inherited Alzheimer Network

[a]Mallinckrodt Institute of Radiology, Washington University School of Medicine, Saint Louis, MO, USA
[b]Banner Alzheimer's Institute, Phoenix, AZ, USA
[c]Division of Biostatistics, Washington University School of Medicine, Saint Louis, MO, USA
[d]Department of Neurology, Washington University School of Medicine, Saint Louis, MO, USA
[e]Dementia Research Centre, UCL Institute of Neurology, London, UK
[f]Department of Neurology, Columbia University Medical Center, New York, NY, USA
[g]Department of Psychiatry, Washington University School of Medicine, Saint Louis, MO, USA
[h]Neuroscience Department Laboratories, Mount Sinai School of Medicine, New York, NY, USA
[i]Department of Radiology, Mayo Clinic, Rochester, MN, USA
[j]Departments of Psychiatry, University of Pittsburgh School of Medicine, Pittsburgh, PA, USA
[k]Department of Radiology, University of Michigan, Ann Arbor, MI, USA
[l]Memory and Aging Center, Department of Neurology, Keck School of Medicine at the University of Southern California, Los Angeles, CA, USA
[m]Center for Neuroimaging, Department of Radiology and Imaging Science, Indiana University School of Medicine, Indianapolis, IN, USA
[n]Laboratory of Neuroimaging, David Geffen School of Medicine, University of California, Los Angeles, CA, USA

**Abstract**

**Introduction:** ^{18}F-fluorodeoxyglucose (FDG) positron emission tomography (PET) is commonly used to estimate neuronal injury in Alzheimer's disease (AD). Here, we evaluate the utility of dynamic PET measures of perfusion using ^{11}C-Pittsburgh compound B (PiB) to estimate neuronal injury in comparison to FDG PET.

**Methods:** FDG, early frames of PiB images, and relative PiB delivery rate constants (PiB-R1) were obtained from 110 participants from the Dominantly Inherited Alzheimer Network. Voxelwise, regional cross-sectional, and longitudinal analyses were done to evaluate the correlation between images and estimate the relationship of the imaging biomarkers with estimated time to disease progression based on family history.

**Results:** Metabolism and perfusion images were spatially correlated. Regional PiB-R1 values and FDG, but not early frames of PiB images, significantly decreased in the mutation carriers with estimated year to onset and with increasing dementia severity.

**Discussion:** Hypometabolism estimated by PiB-R1 may provide a measure of brain perfusion without increasing radiation exposure.

© 2018 The Authors. Published by Elsevier Inc. on behalf of the Alzheimer's Association. This is an open access article under the CC BY-NC-ND license (http://creativecommons.org/licenses/by-nc-nd/4.0/).

*Keywords:* Alzheimer's disease; Neuronal injury; Perfusion; FDG; PiB

*Corresponding author. Tel.: +(602) 839 4851; Fax: +(602) 839 3498.

E-mail address: yi.su@bannerhealth.com

## 1. Introduction

Alzheimer's disease (AD) can be staged with biomarkers including positron emission tomography (PET), magnetic resonance imaging (MRI), and cerebrospinal fluid to detect β-amyloid (Aβ), neurofibrillary tau tangles, and neurodegeneration [1–3]. ^{11}C-Pittsburgh compound B (PiB) PET is commonly used to detect cerebral Aβ burden [4,5]. ^{18}F-fluorodeoxyglucose (FDG) PET is an analogue of glucose that accumulates in brain cells thus allowing visualization and measurement of local metabolic activity. Decrease in FDG uptake is thought to reflect local neuronal dysfunction [6] and is used as a reliable imaging biomarker for AD diagnosis.

Models of AD pathophysiology propose a sequential progression of brain changes that are reflected by imaging abnormalities starting with an early increase in Aβ-PET tracer retention, followed by a decrease in glucose metabolism, followed by a decrease in cortical thickness as seen with volumetric MRI [2,7]. Imaging participants with multiple PET tracers help characterize different stages of the disease but is limited by cumulative radiation exposure, greater participant burden, and increased study costs. To address this, several recent investigations have evaluated perfusion-weighted PET or cerebral blood flow (CBF) as potential estimates of glucose metabolism measurements [8–12]. Good spatial correlations were found between CBF estimates and FDG, including in regions affected by hypometabolism in symptomatic sporadic AD [8,10,12]. The gold standard for CBF measurement is $^{15}O$-$H_2O$ PET [13,14]; however, its 2-minute half-life prevents its widespread use [13]. $^{15}O$-$H_2O$ has been used to validate perfusion weighted measurements derived from PiB PET [15] based upon influx of the PiB tracer into the brain [16] using either the early frames of the PiB scan (ePiB) or a relative tracer influx rate (PiB-R1) [15,17]. Several studies on sporadic AD showed that a perfusion image with ePiB, in addition to a common Aβ burden PiB image, improves discrimination between AD pathology and other Aβ- and tau-related clinical disorders [10,18,19]. ePiB also helps distinguish the earliest symptomatic stage of AD from healthy controls [20]. Another study from Meyer et al. showed that PiB-R1 and FDG images were similar in a population with dementia and suggested that PiB-R1 can be used as a good surrogate for FDG [9].

To our knowledge, changes in PiB-R1 and ePiB with the progression of the disease have not been evaluated either cross-sectionally or longitudinally. Here, we compared PiB-R1 and ePiB with FDG in a model of AD progression to evaluate their utility in clinical research and trials of dynamic Aβ PET measures as markers of neuronal injury. A validation substudy compared PiB-R1 and ePiB with the perfusion gold standard, $^{15}O$-$H_2O$ PET.

We focused on a population with autosomal dominant AD (ADAD) to facilitate the evaluation of disease progression and preclinical AD stages. ADAD is a rare familial form of AD with early onset of clinical symptoms (typically before 65 years old) caused by a mutation in the amyloid precursor protein (APP), presenilin 1 (PS1), or presenilin 2 (PS2) genes, resulting in overproduction of Aβ. These forms of familial AD have essentially 100% penetrance and show similar age of symptom onset in each family across generations [21]. Because the disease course is well characterized, ADAD provides an important model for staging preclinical AD [21]. The Dominantly Inherited Alzheimer Network (DIAN) has described disease progression in ADAD, finding that glucose metabolism is primarily diminished in regions including the precuneus and inferior parietal cortices, beginning ∼10 years before symptom onset [22]. We investigated in an ADAD cohort from the DIAN whether PiB-R1 and ePiB values derived from dynamic PiB PET show similar declines in the parietal and temporal lobes as seen with FDG PET, with the aim to evaluate a potential alternative to the FDG neuronal injury marker of AD that would minimize radiation exposure, experiment time, and participant burden in the context of clinical research and trials.

## 2. Methods

### 2.1. Participants

Participants were enrolled at DIAN sites, including three sites that performed full-dynamic PiB PET scans: Washington University, Columbia University, and University of California Los Angeles. Each site's institutional review board approved all study procedures. All participants or their caregivers provided written informed consent approved by their local institution's review board. Standardized clinical and imaging assessments were obtained according to DIAN study protocols [23]. Data were from the DIAN Data Freeze 7 (May 2014) and had passed strict quality control procedures. This data set included 110 participants with at least one full-dynamic PiB PET scan available for analysis. Sixty-five participants were mutation carriers (MCs) of the genes APP, PS1, or PS2. Forty-five participants with an MC parent were themselves noncarriers (NCs) and were considered as controls (see demographics Table 1). All participants had baseline MRI, PiB, and FDG PET scans, genetic analyses, and clinical assessments using the clinical dementia rating (CDR) with both a global score and a more detailed CDR sum of boxes (CDR-SB) score based on several cognitive and behavioral categories [24,25]. Longitudinal analyses were performed on a subset of 30 participants with at least one follow-up session including dynamic PiB and FDG scans (see demographics in Table 2). Of the 110 participants with baseline dynamic data, 30 participants at the Washington University site additionally underwent an $^{15}O$-$H_2O$ PET scan for CBF assessment (see demographics in Supplementary Table S1).

### 2.2. Image acquisition

Standard procedures were used at all DIAN sites and ensured consistency in the data collection [21,23]. Two

Table 1
Demographics of cross-sectional data

| Parameters | NC | MC | P value |
|---|---|---|---|
| N (%) | 45 (40.9) | 65 (59.1) | - |
| Age, mean (SD) years | 38.2 (10.1) | 39.8 (12.0) | .53 |
| EYO, mean (SD) years | −8.3 (10.6) | −7.8 (11.4) | .95 |
| Education, mean (SD) | 15.0 (2.8) | 15.2 (2.9) | .78 |
| Male, n (%) | 22 (48.9) | 36 (55.4) | .50 |
| CDR > 0, n (%) | 5 (11.1) | 22 (33.8) | .012* |
| MCBP > .18, n (%) | 1 (2.2) | 40 (61.5) | $9.05 \times 10^{-10\dagger}$ |
| MCBP value, mean (SD) | 0.05 (0.1) | 0.38 (0.1) | $8.82 \times 10^{-11\dagger}$ |

Abbreviations: SD, standard deviation; NC, noncarrier; MC, mutation carrier; EYO, estimated year to symptom onset; CDR, clinical dementia rating.

NOTE. In the cross-sectional cohort, the 2 groups, NCs and MCs, were similar in age, EYOs, education score, and gender. The MC group had a significant higher proportion of participants with cognitive impairments (CDR > 0) and amyloid deposition (MCBP > .18).

*P value < .05.
†P value < .0005.

institutions reviewed the scanner parameters, performance, and image quality for the MRI (Mayo Clinic in Rochester) and for the PET (University of Michigan, see Supplementary Fig. S1). The MRI scan consisted of a sagittal 3D T1-weighted image, corresponding to an accelerated magnetization-prepared rapid acquisition with gradient echo (MPRAGE). The MRI was acquired on 3T scanners with the following parameters: TR = 23,000, TE = 2.95, and $1.0 \times 1.0 \times 1.2$ mm$^3$ resolution. The PiB PET scan consisted of 70 minutes of dynamic scanning after an ∼13-mCi bolus injection. The FDG PET scan started 30 minutes after an ∼5-mCi bolus injection and lasted 30 minutes. The $^{15}$O-H$_2$O PET scans started after an ∼50-mCi bolus injection and lasted 3 minutes.

### 2.3. Image processing and image analysis

For each participant, the PET images were processed using regions of interest (ROIs) from FreeSurfer brain segmentation software (http://surfer.nmr.mgh.harvard.edu/)

Table 2
Demographics of longitudinal data at baseline

| Parameters | NC | MC | P value |
|---|---|---|---|
| N (%) | 15 (50) | 15 (50) | - |
| Age, mean (SD) years | 40.5 (7.5) | 41.7 (9.0) | .819 |
| EYO, mean (SD) years | −3.8 (7.6) | −4.2 (6.2) | .983 |
| Education, mean (SD) | 14.7 (2.0) | 14.9 (2.0) | .831 |
| Male, n (%) | 6 (40) | 10 (66.7) | .272 |
| CDR > 0, n (%) | 0 | 7 (46.7) | $9.60 \times 10^{-03}*$ |
| MCBP > .18, n (%) | 1 (6.7) | 12 (80) | $2.29 \times 10^{-04\dagger}$ |
| MCBP value, mean (SD) | 0.09 (0.2) | 0.53 (0.2) | $8.98 \times 10^{-05\dagger}$ |

Abbreviations: SD, standard deviation; NC, noncarrier; MC, mutation carrier; EYO, estimated year to symptom onset; CDR, clinical dementia rating; MCBP, mean cortical binding potential.

NOTE. In the longitudinal cohort, the 2 groups, NCs and MCs, were similar in age, EYOs, education score, and gender. The MC group had a significant higher proportion of subjects with cognitive impairments (CDR > 0) and amyloid deposition (MCBP > .18).

*P value < .01.
†P value < .001.

as previously described [21]. The brainstem was used as reference for PiB and FDG scans, and the whole brain was used as reference for the $^{15}$O-H$_2$O scans. For ROI analyses, all the PET images were corrected for partial volume effects using a regional point spread function [26]. Additional results from noncorrected data were shown in Supplementary Fig. S2. A mean cortical binding potential (MCBP) was calculated from the full-dynamic PiB scan and used to define PiB positivity (MCBP > .18), as previously described [27]. FDG and $^{15}$O-H$_2$O images were quantified as described in previous studies [22,28]. Various spans of sequential early frames of the PiB PET scan were summed to obtain ePiB standardized uptake value ratio (SUVR) images for different time frames (0 to 5, 1 to 6, 1 to 7, 1 to 8, 1 to 9, 1 to 10, and 1 to 12 minutes). The ePiB image that best spatially correlated with FDG (ePiB 1 to 9 minutes) was used for analyses (see Supplementary Table S2 and Fig. S3). PiB-R1 values were derived from the full-PiB dynamic time activity curves using a simplified reference tissue model [29] on a regional basis for each full-dynamic PiB scan to characterize the relative perfusion for a target region versus the reference region [30].

For each participant, voxelwise spatial correlations of the entire brain, cortical, and subcortical deep gray were evaluated between (1) the FDG and $^{15}$O-H$_2$O images; (2) the PiB-R1 and $^{15}$O-H$_2$O images; and (3) ePiB and $^{15}$O-H$_2$O. ROI analyses were done on regions that have shown severe hypometabolism in ADAD: the precuneus and the inferior and superior parietal [22]. Other ROIs with relatively preserved metabolism with ADAD pathology were also evaluated: the lateral occipital and the hippocampus [22]. Note that the ROIs were averaged for the left and right hemispheres. Supplemental voxel-based morphometry analyses were performed to compare gray matter differences between NC and MC participants (Supplementary Fig. S4) [31,32].

### 2.4. Statistical analysis

The cross-sectional relationship of FDG, PiB-R1, and ePiB with the estimated year to symptom onset (EYO) was evaluated per mutation group using general linear mixed-models on each ROI. The models included fixed effects for mutation status, EYO, and the interaction between the mutation status and EYO, and random intercepts at the family level. The potential presence of nonlinear trajectories was examined with the inclusion and testing of quadratic and cubic EYO terms, along with appropriate interaction terms with the mutation status indicator. Owing to the preliminary hypothesis-generating nature of the present study, no adjustment for multiple comparisons was performed.

The relationship with CDR-SB was evaluated across the subset of 65 MCs with Spearman's rank correlation for each region. To evaluate the differences between FDG/CDR-SB, PiB-R1/CDR-SB, and ePiB/CDR-SB, we computed the 95% confidence interval for the difference in

Spearman's rank correlation coefficients based on the percentile method using 10,000 bootstrap replications [33].

For the longitudinal analyses, to quantify the within-person annual rate of change in FDG, PiB-R1, or ePiB, general linear mixed models were used with random intercepts and random slopes at the participant level, along with random effects at the family level. Fixed effects included a mutation status indicator, EYO at baseline, and time from baseline. The interactions between time from baseline and the two other fixed effects were also included.

All general linear mixed models were estimated using restricted maximum likelihood estimation. F-test denominator degrees of freedom were approximated using the Satterthwaite method [34]. All statistical analyses were performed with SAS, version 9.4 (SAS Institute Inc.).

## 3. Results

### 3.1. Participant characteristics

The demographics of the cross-sectional cohort, the longitudinal cohort, and the $^{15}O-H_2O$-PET cohort are summarized in Table 1, Table 2, and Supplementary Table S1, respectively. The NC and MC groups were similar in age, EYO, and education for all cohorts. The two groups were different in CDR and MCBP as expected, with higher prevalence of symptomatic (CDR > 0) and PiB-positive (MCBP > .18) participants in the MC group.

### 3.2. Comparison of perfusion measures and FDG

To test whether FDG, PiB-R1, and ePiB displayed strong perfusion characteristics, we compared these measures with $^{15}O-H_2O$ the gold standard of perfusion, regardless of the mutation status. In the 30 DIAN participants with $^{15}O-H_2O$ data, the spatial average Pearson's r values for FDG, PiB-R1, and ePiB were 0.69 ± 0.05, 0.74 ± 0.09, and 0.71 ± 0.06 for the entire brain, and 0.57 ± 0.04, 0.64 ± 0.10, and 0.58 ± 0.05 for cortical gray matter,

respectively. The average Pearson's r values for the correlation of PiB-R1 and $^{15}O-H_2O$, and of ePiB and $^{15}O-H_2O$, were similar for the entire brain. However, the average Pearson's r value for the correlation of PiB-R1 and $^{15}O-H_2O$ was significantly higher than that of ePiB and $^{15}O-H_2O$ on the cortical level ($P < .0001$). This suggests better perfusion characteristics of the PiB-R1 values.

Visual comparison of the FDG, PiB-R1, ePiB, and Aβ uptake PiB images within participants revealed that PiB-R1 was more similar to FDG than ePiB was (Fig. 1). Across all the 110 participants, the PiB-R1 values better correlated with FDG in the precuneus (r = 0.48, $P < .0001$) and the inferior parietal (r = 0.42, $P < .0001$) than did ePiB values (precuneus: r = 0.08, n.s.; inferior parietal: r = 0.22, n.s.), whereas ePiB correlated better in the hippocampus (r = 0.52, $P < .0001$) than did PiB-R1 (r = 0.40, $P < .0001$) (Fig. 2 and Supplementary Table S3).

### 3.3. Comparison of perfusion measures and MCBP

PiB is a PET ligand designed for imaging cerebral fibrillar Aβ [4]. We tested whether PiB-R1 and ePiB were contaminated by Aβ binding by evaluating their correlation with MCBP. Across all 110 participants, the PiB-R1 values were not correlated with MCBP for all regions. However, ePiB positively correlated with Aβ burden in several regions (e.g., r = 0.59, $P < .0001$; and r = 0.37, $P < .0001$ in the precuneus and the inferior parietal cortex, respectively, Supplementary Fig. S5 and Supplementary Table S4). This demonstrates that ePiB measurement displays some contamination from specific binding, whereas PiB-R1 does not.

### 3.4. Cross-sectional evaluation with estimated year to onset

Results for FDG, PiB-R1, and ePiB in the precuneus, the inferior parietal, and the hippocampus were compared in Fig. 3. Based on cross-sectional regional analyses, the MC participants showed a significant decrease of glucose
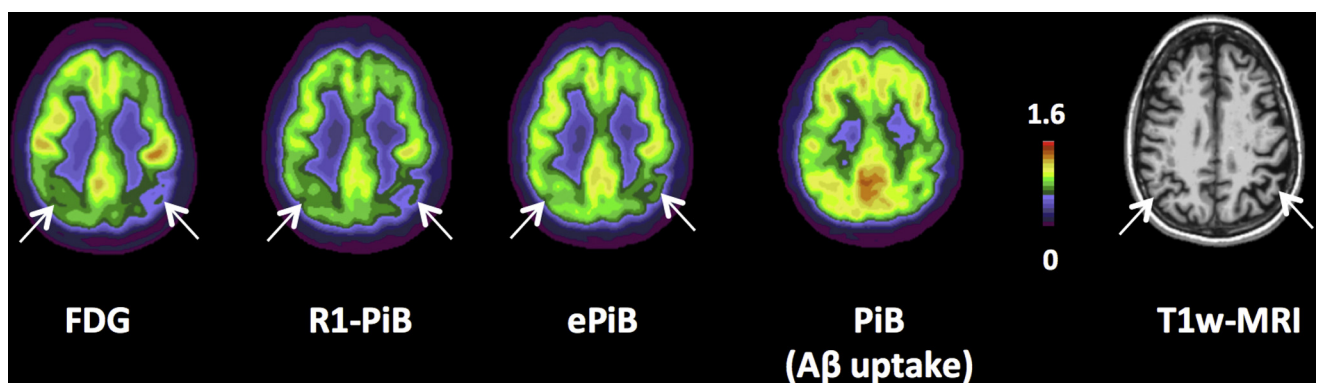


Fig. 1. Multi-imaging modality in a symptomatic mutation carrier. Axial views of FDG, PiB-R1, ePiB (early frames), PiB (β-amyloid uptake), and T1-weighted (T1w-MRI) modalities in one participant carrier of an ADAD mutation. The participant presented a decrease of FDG cerebral glucose metabolism in parieto-temporal areas. PiB-R1 and ePiB image modalities showed decrease signal in matched areas. The PiB image measuring β-amyloid burden did not show same pattern as FDG. Abbreviations: ADAD, autosomal dominant Alzheimer's disease; FDG, $^{18}F$-fluorodeoxyglucose; PiB, $^{11}C$-Pittsburgh compound B; EPiB, early frames of the PiB scan; MRI, magnetic resonance imaging.
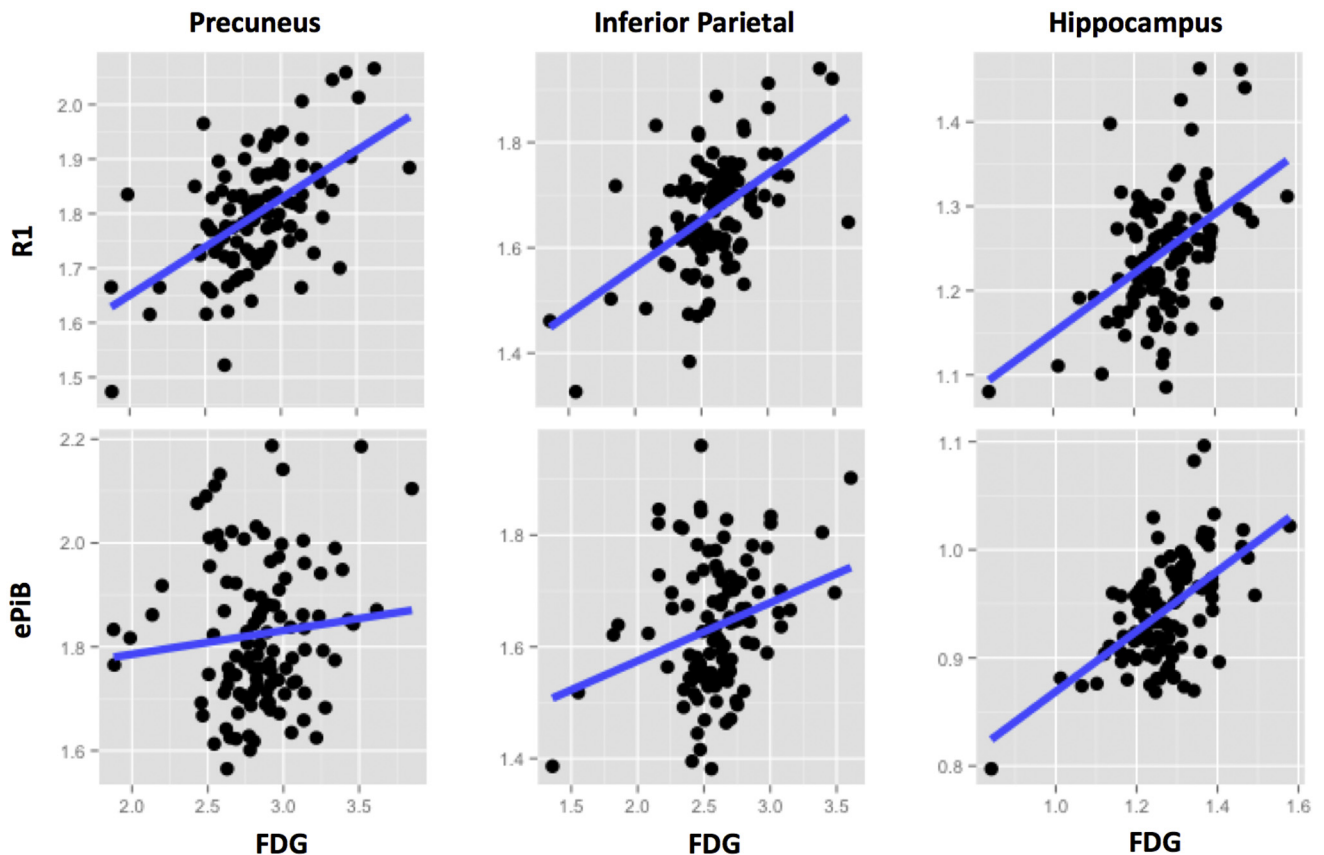
Fig. 2. Comparison of the perfusion models versus FDG across participants. Scatter plots between PiB-R1 and FDG (top), and between ePiB and FDG (bottom) in the precuneus (right panel), the inferior parietal (middle panel), and in the hippocampus (left panel). Across the 110 participants, the PiB-R1 values better correlated with FDG than ePiB values did. Abbreviations: FDG, ^{18}F-fluorodeoxyglucose; PiB, ^{11}C-Pittsburgh compound B; EPiB, early frames of the PiB scan.

metabolism with EYO (all regions, $P < .05$), whereas the NC participants remained stable for all regions (see Fig. 3 top row and Supplementary Table S5). The interaction between mutation and EYO was significant only for the precuneus and the inferior parietal. PiB-R1 decreased for the inferior and superior parietal ($P < .05$) and had a tendency to decrease in the precuneus ($P = .053$) within the MC participants, but the interactions were not significant (see Fig. 3 middle row and Supplementary Table S5). ePiB was significantly increased in the MC population in the precuneus ($P < .0005$), the inferior parietal cortex ($P < .05$), and showed positive interaction in the precuneus (see Fig. 3, bottom row, and Supplementary Table S5).

### 3.5. Cross-sectional evaluation with clinical status

FDG SUVR inversely correlated with the severity of dementia, estimated with CDR-SB, in MC participants (n = 65), with a strong correlation in the precuneus and the inferior and the superior parietal (e.g., rho = $-0.47$, $P < .0001$ for the superior parietal, see Table 3). Similarly, PiB-R1 values were inversely correlated with CDR-SB in all regions except for the lateral occipital and the hippocampus (e.g., rho = $-0.44$, $P < .0005$ for the superior parietal, see Table 3). However, ePiB SUVR values did not significantly correlate with the CDR-SB in any regions (Table 3).

### 3.6. Longitudinal evaluation

Within the MC participants, the longitudinal data demonstrated a significant decrease in FDG in all cortical regions except the lateral occipital and hippocampus (Supplementary Table S6). Similar results were observed for PiB-R1 in the superior parietal, but no significant changes were observed for ePiB within MC participants (Supplementary Table S6). However, examining the differences in slope between MC and NC participants, these changes observed over time in the MC group were not significantly different from the NC group in these regions for all three measurements (Supplementary Table S6).

## 4. Discussion

We demonstrated that PiB-R1, a perfusion-weighted parameter derived from PiB PET, was correlated with FDG and decreased with disease progression in an ADAD population. This was the first study to examine a PET measure of perfusion with disease progression in AD to assess its utility in clinical research and trials as a marker of neuronal injury.

For this purpose, it was necessary to confirm the reliability of our FDG measurements in terms of decreases in our ADAD cohort. Regional hypometabolism begins early in disease
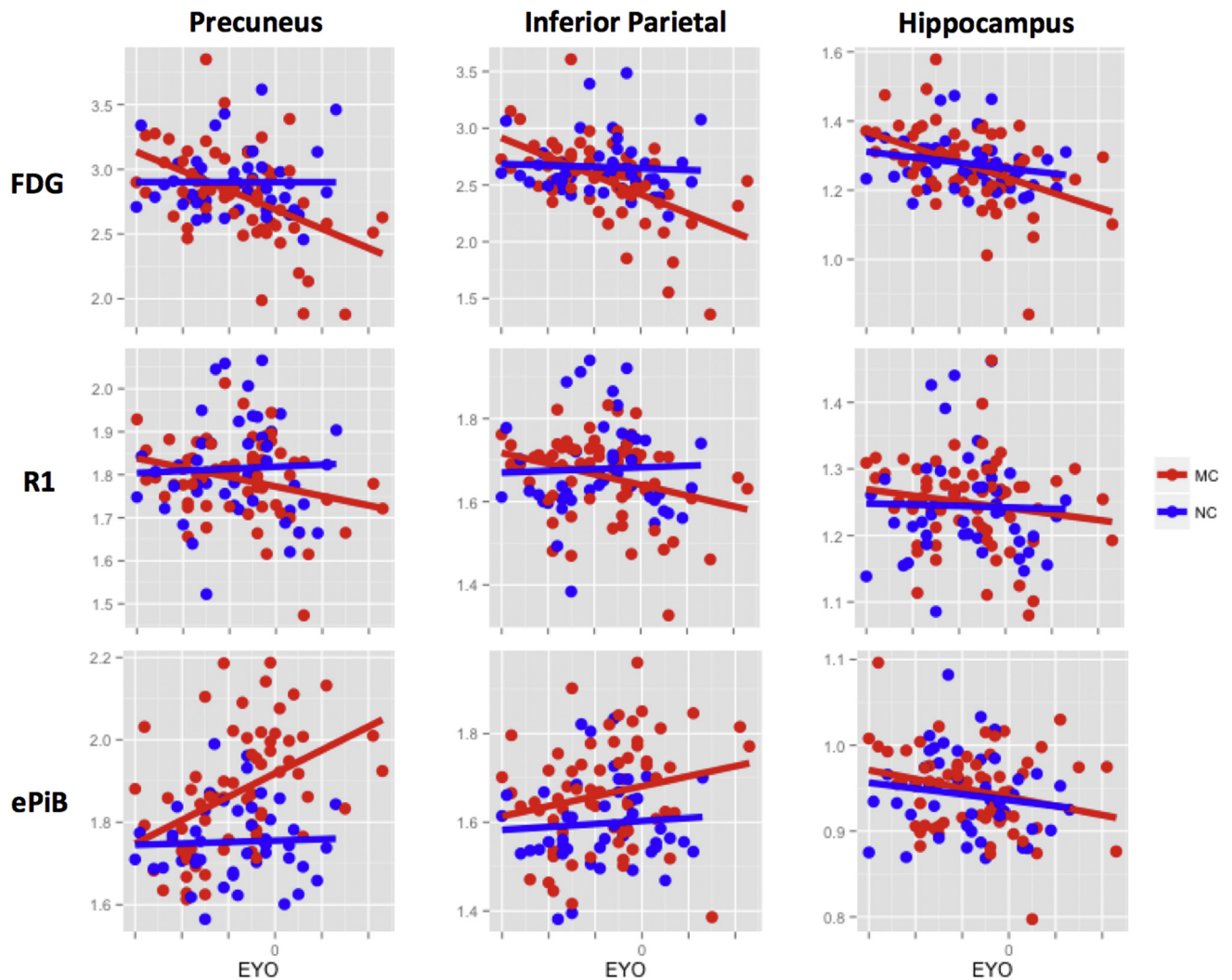
Fig. 3. Progression of FDG, PiB-R1, and ePiB as a function of EYO across mutation carriers. Plots of standardized estimated difference between MC (red) and NC (blue) participants for FDG (top), PiB-R1 (middle), and ePiB (bottom) at different cortical and subcortical levels: precuneus (left panel), inferior parietal (middle panel), and hippocampus (right panel). FDG and ePiB evolved in opposite directions, whereas PiB-R1 and FDG showed both decrease with EYO. Abbreviations: FDG, $^{18}$F-fluorodeoxyglucose; PiB, $^{11}$C-Pittsburgh compound B; EPiB, early frames of the PiB scan; NC, noncarrier; MC, mutation carrier; EYO, estimated year to symptom onset.

progression and can be reliably measured with FDG. Using an ADAD population, it is possible to model the relative progression of the disease with EYO [2,22]. Previous FDG cerebral metabolism findings in ADAD showed decreases, particularly, in the precuneus, parietal, and cingulate areas [2,22]. In the present study, the cortical glucose metabolism decrease was observed in MC participants in both cross-sectional and longitudinal analyses, and this decrease was linked to cognitive impairment. Our findings are consistent with previous studies indicating that FDG glucose metabolism is a sensitive marker of disease progression in ADAD.

When both PiB-R1 and ePiB were compared with FDG from the same participant and visit, PiB-R1 showed a better spatial correlation. Across DIAN participants, the correlations were stronger between PiB-R1 and FDG than ePiB and FDG in most cortical areas. These findings demonstrate that PiB-R1 is better correlated with FDG both within and across subjects and provides a closer proxy of FDG than ePiB. In our study, PiB-R1

values showed greater similarity to FDG during disease progression than did ePiB. First, PiB-R1 decreased in regions such as the inferior and superior parietal with EYO cross-sectionally, whereas ePiB increased with EYO in these regions. Second, decreases in PiB-R1 with CDR-SB were found in all areas greatly affected by hypometabolism, whereas ePiB did not show any interaction with clinical status. Finally, longitudinally, in MC participants, the PiB-R1 measures showed a consistent trend of decrease, which reached significance in the superior parietal, whereas ePiB did not show any significant changes in the MC participants. The evaluated relationships were stronger in parietotemporal areas than in lateral occipital. Early in the disease course, parietotemporal areas are first to show hypometabolism, whereas lateral occipital areas are only affected later [22].

The counterintuitive increase in ePiB with EYO in regions affected by hypometabolism and the lack of decrease with cognitive impairment are consistent with

Table 3
Correlation between tracers and CDR-SB

| Region | FDG and CDR-SB | | PiB-R1 and CDR-SB | | ePiB and CDR-SB | |
|---|---|---|---|---|---|---|
| | rho | P value | rho | P value | rho | P value |
| Precuneus | **−0.45** | **.0001** | **−0.27** | **.029** | 0.17 | .182 |
| Inferior Parietal | **−0.47** | **<.0001** | **−0.28** | **.026** | 0.06 | .650 |
| Superior Parietal | **−0.47** | **<.0001** | **−0.44** | **.0002** | −0.04 | .781 |
| Lateral Occipital | **−0.26** | **.034** | −0.17 | .188 | 0.20 | .103 |
| Hippocampus | **−0.30** | **.014** | −0.22 | .084 | −0.21 | .095 |

Abbreviations: CDR-SB, Clinical Dementia Rating–Sum of Boxes; FDG, $^{18}$F-fluorodeoxyglucose; PiB, $^{11}$C-Pittsburgh compound B; EPiB, early frames of the PiB scan.

NOTE. Statistically significant values are listed in bold ($P$ value <.05).

NOTE. Evaluation of correlation between the tracers and dementia in mutation carriers (n = 65). Spearman's rank correlation coefficient (rho) and $P$ values are displayed for FDG and CDR-SB, ePiB, and CDR-SB, and for PiB-R1 and CDR-SB. There were strong negative correlations between FDG and CDR-SB, but no correlation between ePiB and CDR-SB.

contamination by early binding to Aβ deposits. This early binding caused overestimation of perfusion in ePiB, but not PiB-R1. Different profiles of progression were thus observed between the two perfusion PET measures in the present study. Chen et al. showed that ePiB and PiB-R1 displayed similar spatial profiles [15], but the progression of the disease was not considered. In ADAD, as the disease progresses, the Aβ deposition and thus the MCBP increase [2,22]. The precuneus and the inferior parietal are particularly affected by the increase of Aβ deposition [22]. In the present study, the precuneus and the inferior parietal displayed strong positive correlation between the ePiB measure and MCBP. This may have been due to contamination by Aβ binding, as these increases were not observed in PiB-R1.

Besides Aβ deposition, AD progression is associated with atrophic processes in more advanced stages [1,2,22]. PET SUVR can be strongly affected by atrophic processes, due to the partial volume effect [35,36]. A voxel-based morphometry gray matter comparison between NC and MC participants showed that very few voxels survived correction for multiple comparisons, suggesting that the association observed was not due to differential atrophic process between the groups (Supplemental Fig. S4) [37]. A correction for partial volume effects was applied to our ePiB and PiB-R1 data to obtain a more accurate measure, not contaminated by atrophy. Our group and other groups have shown the importance of partial volume correction (PVC) in PET-image processing [25,38,39]. However, the use of PVC may lead to different outcomes in PET studies [25,40]. Although our main ePiB (corrected) results showed increase with ADAD progression in the MC participants, the same noncorrected data tend to decrease with EYO (see Supplemental Fig. S2). PiB-R1 showed the same trend with or without PVC. Thus, PVC is not necessary for PiB-R1, resulting in simpler processing.

The current results also support the hypothesis that decreases in perfusion and in cerebral glucose metabolism are coupled

during the course of ADAD. However, the findings with the $^{15}$O-H$_2$O subset data confirm that metabolic and perfusion estimates are measuring two different biologic phenomena. Cerebral glucose metabolism may be coupled to CBF in most conditions [41], but the regional variability and relationships with the disease are not clear [42]. Gur et al. found in healthy participants that few cortical areas had coupling between CBF and cerebral glucose metabolism and most cortical and subcortical areas were either hyperperfused or hypoperfused relative to their metabolic values. These observations confirmed that those two measurements are linked but not the same [42].

The results of the present study show clear utility for using the PiB-R1 in clinical research or trials to measure physiologic changes. However, two potential issues can be encountered in practical terms: the dropout rate and the multisite implementation. First, PiB-R1 calculation requires a long scan session that may not be well tolerated by individuals with cognitive impairment. In our study, one out of over 30 participants with follow-up assessments switched to a short protocol. The dropout rate was not an issue in our DIAN longitudinal cohort. Second, not all DIAN sites acquired the full-dynamic scan. Some acquire only a late 30-minute frame beginning 40 minutes after tracer injection. Other sites additionally acquire the first 10 minutes for calculating ePiB in addition to the amyloid load, attempting to minimize study cost and participant burden. Although these approaches decrease the amount of time a participant spends in the scanner, the advantages of PiB-R1 over ePiB lead us to conclude that a full-dynamic acquisition is preferable.

Some studies suggested using other Aβ-PET ligands such as florbetapir [43–45], florbetaben [11,46], or tau PET ligands [17] to measure perfusion and compare with FDG measurements. Further investigation using other PET tracers could be of interest to fully assess the utility of alternative perfusion proxies using PET tracers in an ADAD population.

These perfusion PET imaging modalities do not measure the same feature as FDG but still possess utility for clinical research and trials. This investigation of ePiB and PiB-R1 measures in an ADAD cohort gives a better characterization of alternative measurements and their potential further applications. PiB-R1 may provide a new measure of neuronal injury. Although the current evidence does not suggest that PiB-R1 is a better measure of neuronal injury than FDG, for participants already receiving a PiB PET scan for assessment of Aβ deposition, substitution of PiB-R1 for FDG would minimize radiation exposure, experiment time, and participant burden by acting as a surrogate for the FDG scan without causing significant dropout on longitudinal follow-up visits during clinical research and trials. Further study evaluating the applicability of PiB-R1 in sporadic AD and other conditions is of interest.

## Supplementary data

Supplementary data to this article can be found online at https://doi.org/10.1016/j.dadm.2018.08.012.

## RESEARCH IN CONTEXT

1. Systematic review: The literature was reviewed using PubMed. Use of PiB PET to assess perfusion in addition to measure brain β-amyloid burden has been recently investigated in sporadic Alzheimer's disease (AD).

2. Interpretation: In an autosomal dominant AD cohort, we found that the relative tracer delivery rate constant from full-dynamic PiB PET imaging (PiB-R1) behaved similarly to $^{18}$F-fluorodeoxyglucose (FDG) positron emission tomography (PET) and decreased with dementia, whereas early frames of PiB scans (ePiB) that has been proposed as a surrogate for FDG PET in studies of AD did not. This suggests that PiB-R1 is a better proxy for FDG in autosomal dominant AD.

3. Future directions: Implementation of full-dynamic β-amyloid PET scans may improve clinical research in AD, as R1 and β-amyloid burden can be extracted from the same imaging scan session, eliminating the FDG PET session and thus decreasing radiation exposure, participant burden, experiment duration, and study costs.

## References

[1] Jack CR Jr, Knopman DS, Jagust WJ, Petersen RC, Weiner MW, Aisen PS, et al. Tracking pathophysiological processes in Alzheimer's disease: an updated hypothetical model of dynamic biomarkers. Lancet Neurol 2013;12:207–16.
[2] Bateman RJ, Xiong C, Benzinger TL, Fagan AM, Goate A, Fox NC, et al. Clinical and biomarker changes in dominantly inherited Alzheimer's disease. N Engl J Med 2012;367:795–804.
[3] Fagan AM, Holtzman DM. Cerebrospinal fluid biomarkers of Alzheimer's disease. Biomark Med 2010;4:51–63.
[4] Klunk WE, Engler H, Nordberg A, Wang Y, Blomqvist G, Holt DP, et al. Imaging brain amyloid in Alzheimer's disease with Pittsburgh Compound-B. Ann Neurol 2004;55:306–19.
[5] Rowe CC, Ng S, Ackermann U, Gong SJ, Pike K, Savage G, et al. Imaging beta-amyloid burden in aging and dementia. Neurology 2007;68:1718–25.
[6] Mosconi L, Berti V, Glodzik L, Pupi A, De Santi S, de Leon MJ. Pre-clinical detection of Alzheimer's disease using FDG-PET, with or without amyloid imaging. J Alzheimers Dis 2010;20:843–54.
[7] Jack CR Jr, Knopman DS, Jagust WJ, Shaw LM, Aisen PS, Weiner MW, et al. Hypothetical model of dynamic biomarkers of the Alzheimer's pathological cascade. Lancet Neurol 2010;9:119–28.
[8] Forsberg A, Engler H, Blomquist G, Langstrom B, Nordberg A. The use of PIB-PET as a dual pathological and functional biomarker in AD. Biochim Biophys Acta 2012;1822:380–5.
[9] Meyer PT, Hellwig S, Amtage F, Rottenburger C, Sahm U, Reuland P, et al. Dual-biomarker imaging of regional cerebral amyloid load and neuronal activity in dementia with PET and 11C-labeled Pittsburgh compound B. J Nucl Med 2011;52:393–400.
[10] Rostomian AH, Madison C, Rabinovici GD, Jagust WJ. Early 11C-PIB frames and 18F-FDG PET measures are comparable: A study validated in a cohort of AD and FTLD patients. J Nucl Med 2011;52:173–9.
[11] Tiepolt S, Hesse S, Patt M, Luthardt J, Schroeter ML, Hoffmann KT, et al. Early [(18)F]florbetaben and [(11)C]PiB PET images are a surrogate biomarker of neuronal injury in Alzheimer's disease. Eur J Nucl Med Mol Imaging 2016;43:1700–9.
[12] Fu L, Liu L, Zhang J, Xu B, Fan Y, Tian J. Comparison of dual-biomarker PIB-PET and dual-tracer PET in AD diagnosis. Eur Radiol 2014;24:2800–9.
[13] Raichle ME, Martin WR, Herscovitch P, Mintun MA, Markham J. Brain blood flow measured with intravenous H2(15)O. II. Implementation and validation. J Nucl Med 1983;24:790–8.
[14] Frackowiak RS, Lenzi GL, Jones T, Heather JD. Quantitative measurement of regional cerebral blood flow and oxygen metabolism in man using 15O and positron emission tomography: Theory, procedure, and normal values. J Comput Assist Tomogr 1980;4:727–36.
[15] Chen YJ, Rosario BL, Mowrey W, Laymon CM, Lu X, Lopez OL, et al. Relative 11C-PiB Delivery as a Proxy of Relative CBF: Quantitative Evaluation Using Single-Session 15O-Water and 11C-PiB PET. J Nucl Med 2015;56:1199–205.
[16] Blomquist G, Engler H, Nordberg A, Ringheim A, Wall A, Forsberg A, et al. Unidirectional Influx and Net Accumulation of PIB. Open Neuroimag J 2008;2:114–25.
[17] Rodriguez-Vieitez E, Leuzy A, Chiotis K, Saint-Aubert L, Wall A, Nordberg A. Comparability of [18F]THK5317 and [11C]PIB blood flow proxy images with [18F]FDG positron emission tomography in Alzheimer's disease. J Cereb Blood flow Metab 2016;37:740–9.
[18] Liu L, Fu L, Zhang X, Zhang J, Zhang X, Xu B, et al. Combination of dynamic (11)C-PIB PET and structural MRI improves diagnosis of Alzheimer's disease. Psychiatry Res 2015;233:131–40.
[19] Farid K, Hong YT, Aigbirhio FI, Fryer TD, Menon DK, Warburton EA, et al. Early-Phase 11C-PiB PET in amyloid angiopathy-related symptomatic cerebral hemorrhage: Potential diagnostic value? PLoS One 2015;10:e0139926.

[20] Gietl AF, Warnock G, Riese F, Kalin AM, Saake A, Gruber E, et al. Regional cerebral blood flow estimated by early PiB uptake is reduced in mild cognitive impairment and associated with age in an amyloid-dependent manner. Neurobiol Aging 2015;36:1619–28.

[21] Bateman RJ, Aisen PS, De Strooper B, Fox NC, Lemere CA, Ringman JM, et al. Autosomal-dominant Alzheimer's disease: A review and proposal for the prevention of Alzheimer's disease. Alzheimers Res Ther 2011;3:1.

[22] Benzinger TL, Blazey T, Jack CR Jr, Koeppe RA, Su Y, Xiong C, et al. Regional variability of imaging biomarkers in autosomal dominant Alzheimer's disease. Proc Natl Acad Sci U S A 2013;110:E4502–9.

[23] Morris JC, Aisen PS, Bateman RJ, Benzinger TL, Cairns NJ, Fagan AM, et al. Developing an international network for Alzheimer research: The Dominantly Inherited Alzheimer Network. Clin Investig 2012;2:975–84.

[24] Berg L, Miller JP, Storandt M, Duchek J, Morris JC, Rubin EH, et al. Mild senile dementia of the Alzheimer type: 2. Longitudinal assessment. Ann Neurol 1988;23:477–84.

[25] Morris JC. The Clinical Dementia Rating (CDR): current version and scoring rules. Neurology 1993;43:2412–4.

[26] Su Y, Blazey TM, Snyder AZ, Raichle ME, Marcus DS, Ances BM, et al. Partial volume correction in quantitative amyloid imaging. NeuroImage 2015;107:55–64.

[27] Morris JC, Roe CM, Xiong C, Fagan AM, Goate AM, Holtzman DM, et al. APOE predicts amyloid-beta but not tau Alzheimer pathology in cognitively normal aging. Ann Neurol 2010;67:122–31.

[28] Vaishnavi SN, Vlassenko AG, Rundle MM, Snyder AZ, Mintun MA, Raichle ME. Regional aerobic glycolysis in the human brain. Proc Natl Acad Sci U S A 2010;107:17757–62.

[29] Lammertsma AA, Hume SP. Simplified reference tissue model for PET receptor studies. NeuroImage 1996;4:153–8.

[30] Lopresti BJ, Klunk WE, Mathis CA, Hoge JA, Ziolko SK, Lu X, et al. Simplified quantification of Pittsburgh Compound B amyloid imaging PET studies: A comparative analysis. J Nucl Med 2005;46:1959–72.

[31] Ashburner J, Friston KJ. Unified segmentation. NeuroImage 2005; 26:839–51.

[32] Ashburner J, Friston KJ. Diffeomorphic registration using geodesic shooting and Gauss-Newton optimisation. NeuroImage 2011;55:954–67.

[33] Rindskopf D. An introduction to the bootstrap. Efron B, Tibshirani RJ, eds. J Educ Behav Stat. 1997;22:245.

[34] Satterthwaite FE. An approximate distribution of estimates of variance components. Biometrics 1946;2:110–4.

[35] Ibanez V, Pietrini P, Alexander GE, Furey ML, Teichberg D, Rajapakse JC, et al. Regional glucose metabolic abnormalities are not the result of atrophy in Alzheimer's disease. Neurology 1998; 50:1585–93.

[36] Meltzer CC, Zubieta JK, Brandt J, Tune LE, Mayberg HS, Frost JJ. Regional hypometabolism in Alzheimer's disease as measured by positron emission tomography after correction for effects of partial volume averaging. Neurology 1996;47:454–61.

[37] Cash DM, Ridgway GR, Liang Y, Ryan NS, Kinnunen KM, Yeatman T, et al. The pattern of atrophy in familial Alzheimer disease: Volumetric MRI results from the DIAN study. Neurology 2013; 81:1425–33.

[38] Brendel M, Hogenauer M, Delker A, Sauerbeck J, Bartenstein P, Seibyl J, et al. Improved longitudinal [(18)F]-AV45 amyloid PET by white matter reference and VOI-based partial volume effect correction. NeuroImage 2015;108:450–9.

[39] Thomas BA, Erlandsson K, Modat M, Thurfjell L, Vandenberghe R, Ourselin S, et al. The importance of appropriate partial volume correction for PET quantification in Alzheimer's disease. Eur J Nucl Med Mol Imaging 2011;38:1104–19.

[40] Greve DN, Salat DH, Bowen SL, Izquierdo-Garcia D, Schultz AP, Catana C, et al. Different partial volume correction methods lead to different conclusions: An (18)F-FDG-PET study of aging. NeuroImage 2016;132:334–43.

[41] Paulson OB, Hasselbalch SG, Rostrup E, Knudsen GM, Pelligrino D. Cerebral blood flow response to functional activation. J Cereb Blood flow Metab 2010;30:2–14.

[42] Gur RC, Ragland JD, Reivich M, Greenberg JH, Alavi A, Gur RE. Regional differences in the coupling between resting cerebral blood flow and metabolism may indicate action preparedness as a default state. Cereb Cortex 2009;19:375–82.

[43] Hsiao IT, Huang CC, Hsieh CJ, Hsu WC, Wey SP, Yen TC, et al. Correlation of early-phase 18F-florbetapir (AV-45/Amyvid) PET images to FDG images: preliminary studies. Eur J Nucl Med Mol Imaging 2012;39:613–20.

[44] Kuo HC, Hsiao IT, Hsieh CJ, Huang CY, Huang KL, Wai YY, et al. Dual-phase 18F-florbetapir positron emission tomography in patients with primary progressive aphasia, Alzheimer's disease, and healthy controls: A preliminary study. J Formos Med Assoc 2017;116:964–72.

[45] Lin KJ, Hsiao IT, Hsu JL, Huang CC, Huang KL, Hsieh CJ, et al. Imaging characteristic of dual-phase (18)F-florbetapir (AV-45/Amyvid) PET for the concomitant detection of perfusion deficits and beta-amyloid deposition in Alzheimer's disease and mild cognitive impairment. Eur J Nucl Med Mol Imaging 2016;43:1304–14.

[46] Daerr S, Brendel M, Zach C, Mille E, Schilling D, Zacherl MJ, et al. Evaluation of early-phase [18F]-florbetaben PET acquisition in clinical routine cases. NeuroImage Clin 2017;14:77–86.